

Article

DFT Insights into the Hydrodenitrogenation and Ring-Opening of Indole on an M (M = Ni, Pt, Ni–Pt) Slab Model

Cuiping Wang ^{1,*}, Jinpeng Chu ¹, Lianji Zhang ¹, Yan Huang ¹, Zhiqiang Zhang ¹, Hao Chen ² and Hongqi Shi ²

¹ Key Laboratory for Functional Material, Educational Department of Liaoning Province, University of Science and Technology Liaoning, Anshan 114051, China; chujinpeng@ustl.edu.cn (J.C.); zhanglianji@ustl.edu.cn (L.Z.); huangyan@ustl.edu.cn (Y.H.); zhangzhiqiang@ustl.edu.cn (Z.Z.)

² Wuhan Second Ship Design and Research Institute, Wuhan 430064, China; 19chenhao86@163.com or chenhao@csic719.cn (H.C.); shi_hong_qi163.com or shq@csic719.cn (H.S.)

* Correspondence: cuiping1025@ustl.edu.cn

Abstract: Density functional theory (DFT) calculation has been used to study the hydrodenitrogenation (HDN) and ring-opening of indole on an M (M = Ni, Pt, Ni–Pt) slab surface. The possible reaction pathway of indole hydrogenation has been investigated in order to reveal the bimetallic synergistic effects of an M slab surface. Compared to the mechanism of indole hydrogenation on an M slab surface, it was found that a PtNi(111) surface favors indole hydrogenation. According to the results of DFT calculation, it suggests that the bimetallic effect of the M surface plays an important role in indole hydrogenation.

Keywords: density functional theory; indole hydrodenitrogenation; M slab model



Citation: Wang, C.; Chu, J.; Zhang, L.; Huang, Y.; Zhang, Z.; Chen, H.; Shi, H. DFT Insights into the Hydrodenitrogenation and Ring-Opening of Indole on an M (M = Ni, Pt, Ni–Pt) Slab Model. *Symmetry* **2021**, *13*, 1950. <https://doi.org/10.3390/sym13101950>

Academic Editors: Radomir Jasiński and Jan Awrejcewicz

Received: 25 July 2021

Accepted: 25 September 2021

Published: 16 October 2021

Publisher's Note: MDPI stays neutral with regard to jurisdictional claims in published maps and institutional affiliations.



Copyright: © 2021 by the authors. Licensee MDPI, Basel, Switzerland. This article is an open access article distributed under the terms and conditions of the Creative Commons Attribution (CC BY) license (<https://creativecommons.org/licenses/by/4.0/>).

1. Introduction

With increasingly stringent vehicle emissions standards, and a growing requirement for clean and green energies to be improved, refineries must strive to produce qualified products, such as ultra-low sulfur diesel, by removing sulfur, nitrogen and oxygen from heavier, lower-quality feedstocks. However, S-compounds in the desulfurization process compete with N-compounds which also exist in feedstocks. Therefore, it is necessary to carry out the denitrification process before desulfurization in order to avoid the inhibition of catalyst activity due to the competition between N-compounds and S-compounds. For N-compounds in inferior feedstock, catalytic hydrodenitrogenation (HDN) is a promising process to produce renewable, clean and high-quality fuel. In recent decades, transition metals have performed spectacular catalytic activities for HDN because of their unique chemical and physical properties, which have attracted considerable attention from researchers. These transition metals are highly capable of adsorbing hydrogen, which is good for activation and transition of the reactant molecules. Based on these properties, these transition metals show good catalytic performance in activity, selectivity and poison resistance.

The early literature suggests that noble metals have good HDN activities because of providing abundant active hydrogen species [1,2]. In numerous works, noble metals, either alone or as a promoter, can provide effective active sites for adsorption of N-compounds [3]. The dispersion of noble metals in the metallic state plays a pivotal role in C–N cleavage [2,4]. Pt metal sites are especially in favor of hydrodenitrogenation [5]. Molina et al. suggested that metallic Pt acts as an active hydrogen site which has a promotional effect for HDN [3]. Pt/NaY catalysts with synergistic effect of Pt atom and support can achieve a high conversion of quinolone HDN [6]. These works show Pt-based catalysts have good potential for application in HDN [7].

However, noble metallic catalysts are hard to widely apply because of their expensive cost. One method of reducing the catalyst cost is to use a bimetallic catalyst by doping noble metal into non-noble metal [8]. Elliott and co-researchers found that doping Ru into Ni can

enhance the activity and life of catalysts in a HDN reaction [8]. Hirschon's group suggested the synergistic effect of Rh and Co on HDN, which can improve catalytic activity [9]. Guo et al. found that doping Ru into Ni can enhance catalytic activity for HDN. In addition, the ring opening reaction is most effective when catalysts are bifunctional [10,11]. Mcviker et al. studied selective ring opening by bifunctional catalyst [10]. An effective acidity function accompanied with a high-activity hydrogenolysis metal, such as Ir and Pt, results in a bifunctional catalyst system which is much better than conventional hydrocracking catalysts for the selective conversion of naphthenes to alkanes. Atsumi's group and Ding's group found an Ni-based catalyst is beneficial for Ring open reaction because of its effective acidity function [12,13].

Indole, with benzene ring and heterocyclic N-containing compounds [14–16], is extracted from nitrogen-rich biomass by hydrothermal liquefaction [17,18]. In order to improve the combustion value of indole, it is necessary to convert indole into alkanes by denitrication and ring opening reactions. Based on prior works [18–20], noble metal catalysts, such as Pt, are good for hydrogenation reactions, while the catalysts with an acidity function, such as Ni, are good for ring opening reactions. As mentioned above, it has been reported that Pt and Ni experimentally presented high catalytic activity for indole hydrodenitrogenation. A great deal of literature [21,22] about HDN and ring opening mechanism on monometallic catalysts was investigated by DFT. However, the synergistic effect of bimetallic catalysts is still not clear. In addition, a Ni–Pt bimetallic catalyst for indole hydrodenitrogenation has not been reported as far as we know. In this work, we studied the reaction mechanism of indole hydrodenitrogenation and ring-opening on M (M = Ni, Pt, Ni–Pt) slab model by DFT calculation. The calculated results revealed the mechanisms of the indole hydrodenitrogenation reaction on the M slab surfaces, which provide a better understanding from a microscopic perspective.

2. Computational Methodology

The DMol3 code in Materials Studio is applied to calculate all the DFT work. In this paper, the exchange-correlation energy is calculated by the Perdew–Burke–Ernzerf (PBE) functional with a generalized gradient approximation (GGA). The localized double-numerical quality basis was set as DNP to calculate the wave functions. The effective core potential (ECP) was applied to simulate the core electrons of the metal atoms. The k-point mesh was $3 \times 3 \times 1$ and the thermal smearing was 0.005 hartree. The convergences of the energy, maximum force and a maximum displacement were set as 2.0×10^{-5} Ha, 0.004 Ha/Å and 0.005 Å, respectively. The van der Waals (vdW) interactions were performed by the empirical correction scheme of Grimme (DFT-D).

All the transition states (TS) of the elementary reactions, starting from reactant to product, were carried out using a complete linear synchronous transit and quadratic synchronous transit (LST/QST) approach. The methods of linear synchronous transit and quadratic synchronous transit (LST/QST) were applied to calculate the transition states (TS) of the elementary reactions. In addition, the imaginary frequency calculations were carried out to optimize every transition states.

The adsorption energy (E_{ads}) for adsorbate on M surfaces was calculated as follows:

$$E_{ads} = E_{A/M} - E_M - E_{A(g)} \quad (1)$$

where $E_{A/M}$ is the total energy of M surface with an adsorbate; E_M is the energy of the M surface; $E_{A(g)}$ is the energy of the adsorbate in gas-phase.

The activation energy (E_a) and reaction energy (ΔE)

$$E_a = E_{TS} - E_{IS} \quad (2)$$

$$\Delta E = E_{FS} - E_{IS} \quad (3)$$

where E_{TS} is the energy of the transition state; E_{IS} is the energy of the initial state; E_{FS} is the energy of the final state.

All the chemicals involved in indole hydrodenitrogenation are abbreviated and listed in Table 1

Table 1. Nomenclature of chemicals.

Name	Abbreviation	Structural Formula
Indole	IND	C ₈ H ₇ N
1H-Indole,4,5,6,7-tetrahydro	INDTE	C ₈ H ₁₃ N
Indoline	DHIND	C ₈ H ₉ N
Octahydroindole	OHIND	C ₈ H ₁₅ N
o-ethylcyclohexylamine	OECHA	C ₈ H ₁₇ N
Ethylcyclohexane	ECH	C ₈ H ₁₆

3. Results and Discussion

3.1. M Slab Model

Four surface models of M (M = Ni, Pt, NiPt, PtNi) slab were constructed. The calculated lattice constant of bulk Ni and Pt was, respectively, 3.54 Å and 3.91 Å, which are in good agreement with the previous experimental value of 3.53 Å and 3.92 Å, respectively. The Ni(111) surface model and the Pt(111) surface model are shown in Figure 1a,b, respectively. The NiPt(111) surface model is constructed as Ni atom doping into the Pt(111) surface in Figure 1c, while the PtNi(111) surface is constructed as a Pt atom doping into the Ni(111) surface in Figure 1d. In Figure 1a–d, a four-layer symmetric periodic slab was optimized, in which the bottom two layers were fixed at their original atomic positions, and the upper two layers and the adsorbates were allowed to relax during structural optimization. The crystal face of an M slab surface is an M(111) surface with a 3 × 3 surface unit cell. The vacuum thickness is set as 12 Å, which separates the interactions of the periodically slabs.

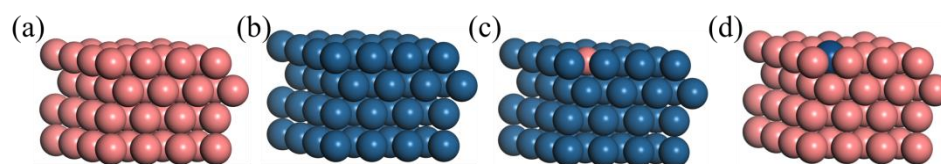


Figure 1. M slab models: (a) Ni(111) surface; (b) Pt(111) surface; (c) NiPt(111) surface; (d) PtNi(111) surface.

3.2. The Adsorption of Indole and Intermediates on M Slab

It is important to study the adsorption structures of reactive species to investigate the elementary steps in indole hydrodenitrogenation reaction. The adsorption structures of indole, octahydroindole and H on M slab were optimized and shown in Figures 2–5. The corresponding adsorption energies are listed in Table 2.

Table 2. Adsorption energies of indole, octahydroindole and H on Ni(111) surface, Pt(111) surface, NiPt(111) surface and PtNi(111) surface.

Configurations	Adsorption Energy (eV)			
	Ni(111)	Pt(111)	NiPt(111)	PtNi(111)
(a)	−1.06	−1.21	−1.25	−1.13
(b)	−2.13	−2.29	−2.36	−2.21
(c)	−1.87	−1.96	−2.09	−1.77
(d)	−1.05	−1.23	−1.11	−1.27
(e)	−1.29	−1.45	−1.32	−1.49
(f)	−0.59	−0.70	−0.68	−0.66
(g)	−0.73	−0.87	−0.93	−0.77
(h)	−2.10	−2.77	−2.81	−2.13
(i)	−2.14	−2.80	−2.69	−2.61
(j)	−2.19	−2.82	−2.54	−2.66
(k)	−2.21	−2.88	−2.59	−2.72

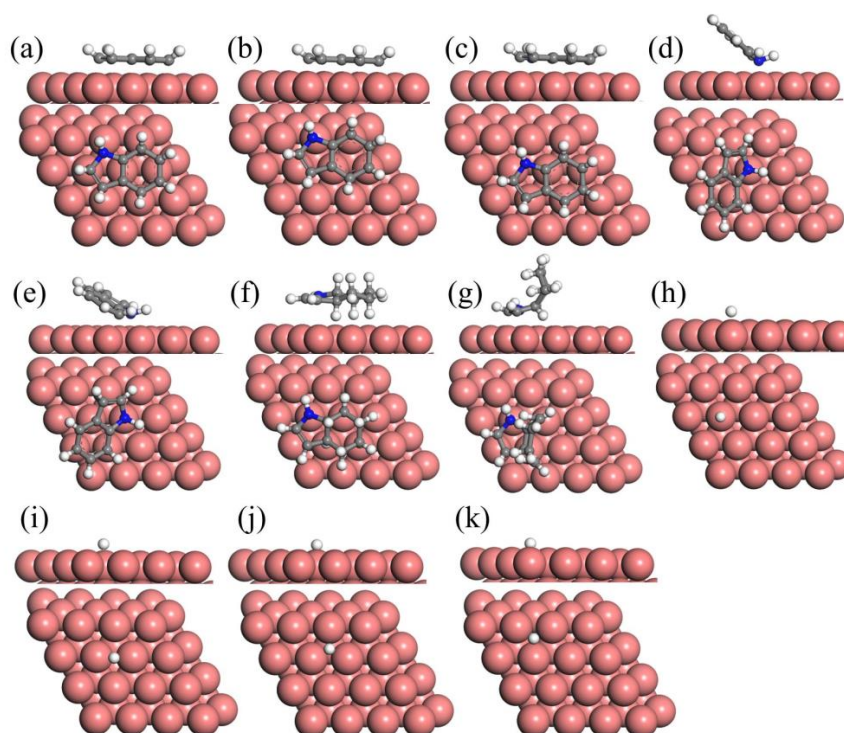


Figure 2. Adsorption configuration of indole, octahydroindole and H on Ni(111) surface: (a) indole adsorption on bridge site; (b) indole adsorption on hcp site; (c) indole adsorption on fcc site; (d) indole adsorption on top site 1; (e) indole adsorption on top site 2; (f) INDTE flat adsorption; (g) INDTE chair adsorption; (h) H adsorption on top site; (i) H adsorption on bridge site; (j) H adsorption on hcp site; (k) H adsorption on fcc site.

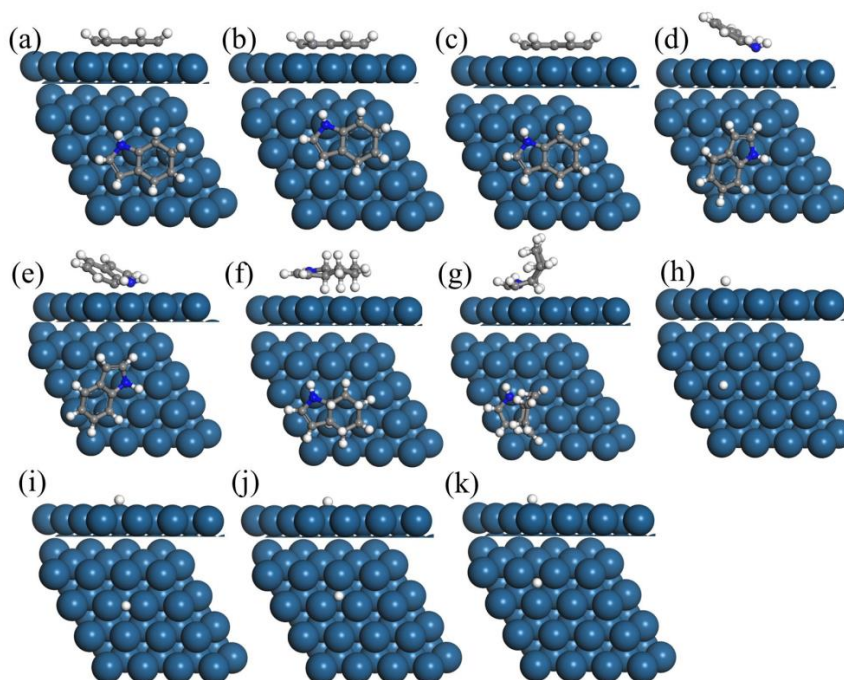


Figure 3. Adsorption configuration of indole, octahydroindole and H on Pt(111) surface: (a) indole adsorption on bridge site; (b) indole adsorption on hcp site; (c) indole adsorption on fcc site; (d) indole adsorption on top site 1; (e) indole adsorption on top site 2; (f) INDTE flat adsorption; (g) INDTE chair adsorption; (h) H adsorption on top site; (i) H adsorption on bridge site; (j) H adsorption on hcp site; (k) H adsorption on fcc site.

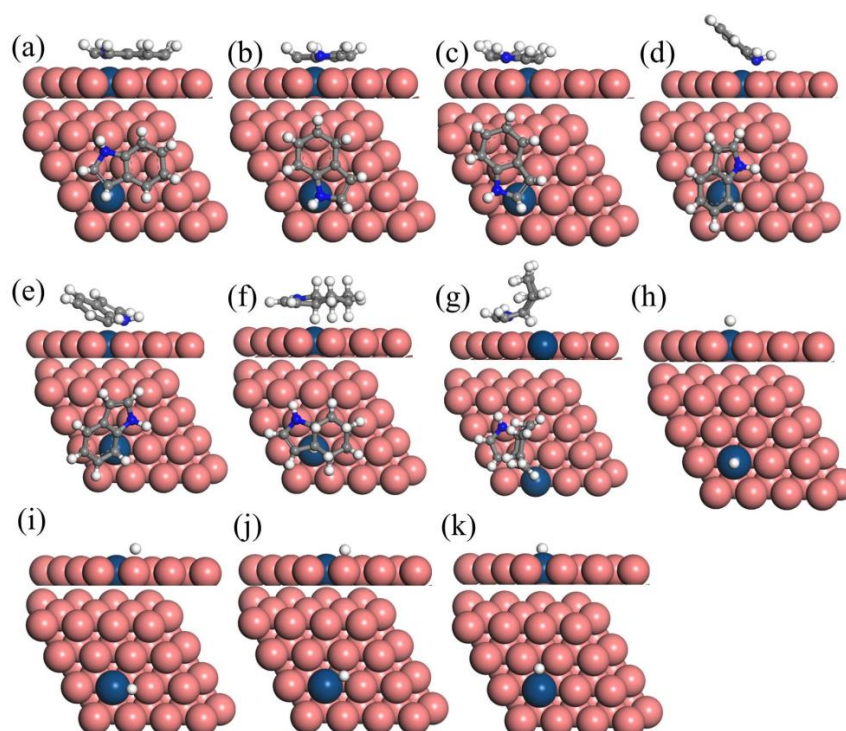


Figure 4. Adsorption configuration of indole, octahydroindole and H on NiPt(111) surface: (a) indole adsorption on bridge site; (b) indole adsorption on hcp site; (c) indole adsorption on fcc site; (d) indole adsorption on top site 1; (e) indole adsorption on top site 2; (f) INDTE flat adsorption; (g) INDTE chair adsorption; (h) H adsorption on top site; (i) H adsorption on bridge site; (j) H adsorption on hcp site; (k) H adsorption on fcc site.

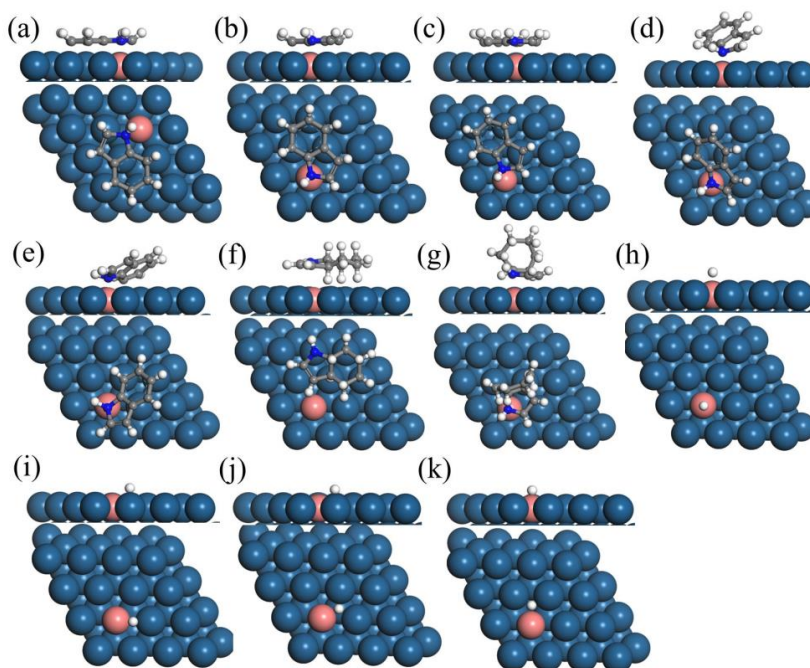


Figure 5. Adsorption configuration of indole, octahydroindole and H on PtNi(111) surface: (a) indole adsorption on bridge site; (b) indole adsorption on hcp site; (c) indole adsorption on fcc site; (d) indole adsorption on top site 1; (e) indole adsorption on top site 2; (f) INDTE flat adsorption; (g) INDTE chair adsorption; (h) H adsorption on top site; (i) H adsorption on bridge site; (j) H adsorption on hcp site; (k) H adsorption on fcc site.

3.2.1. Indole Adsorption on M Slab

Indole interacts with several surface atoms upon adsorption, with the main binding interaction between the aromatic π electrons and the metal surface states. The adsorption configurations of indole on the four M(111) surface are shown in configuration (a), (b), (c), (d) and (e) of Figures 2–5. Configuration (a), (b), (c), (d) and (e) present indole adsorption on bridge site, hcp site, fcc site, top site 1 and top site 2 of the M(111) surface, respectively. In Table 1, the bridge adsorption energy, hcp adsorption energy, fcc adsorption energy, top adsorption energy 1 and top adsorption energy 2 on the Ni(111) surface are -1.06 , -2.13 , -1.87 , -1.05 and -1.29 eV, respectively. On the Pt(111) surface, the adsorption energies of configuration (a), (b), (c), (d) and (e) are lower than that of the corresponding configuration on the Ni(111) surface. The bridge adsorption energy, hcp adsorption energy, fcc adsorption energy, top adsorption energy 1 and top adsorption energy 2 on the Pt(111) surface are -1.21 , -2.29 , -1.96 , -1.23 and -1.45 eV, respectively. On the NiPt(111) surface, the adsorption energies of configuration (a), (b), (c), (d) and (e) are -1.25 , 2.36 , 2.09 , -1.11 and -1.32 eV, respectively. On the PtNi(111) surface, the adsorption energies of configuration (a), (b), (c), (d) and (e) are -1.13 , 2.21 , 1.77 , -1.27 and -1.49 eV, respectively. According to the adsorption energies, the configuration (b) of indole adsorption is the most stable configuration, regardless of the adsorption surfaces. Compared to the adsorption energies of the four surfaces, the indole adsorption energy on the PtNi(111) surface are lowest. This suggests indole adsorbs on the PtNi(111) surface are more stable than that on the other surfaces.

3.2.2. Octahydroindole Adsorption on M Slab

Octahydroindole is the important intermediate in indole hydrodenitrogenation. We considered two adsorption configurations of INDTE adsorption on the four M(111) surface. For configuration (f) in Figures 2–5, INDTE flatly adsorbs on the M(111) surface with adsorption energies in the range between -0.59 and -0.70 eV. For configuration (g) in Figures 2–5, INDTE adsorbs like a chair on the M(111) surface. The adsorption energies of configuration (g) are in the range between -0.77 and -0.93 eV, which are lower than that on the corresponding surface. The adsorption energy of configuration (g) is lower than that of configuration (f), which suggests INDTE prefers to adsorb on the M(111) surface by chair conformation. In addition, the adsorption energy of chair conformation on the PtNi(111) surface is lower than that on the other surface. It suggests INDTE adsorption on the PtNi(111) bimetallic surface is stronger than that on the other surfaces.

3.2.3. H Adsorption on M Slab

We studied the H atom adsorption on the four M(111) surface. Four adsorption sites, top, bridge, fcc and hcp, were considered on M(111) surfaces. The adsorption energies are listed in Table 2. According to the calculation result of four surfaces, it suggests the H atom prefers to adsorb on the Pt(111) surface because of low adsorption energies. In addition, fcc site of the Pt(111) surface is favorable for H adsorption with a lowest adsorption energy of -2.88 eV. For the Ni(111) surface, Pt(111) surface and NiPt(111) surface, the adsorption energies follow the order Top site > Bridge site > Hcp site > Fcc site. However, the adsorption energies of the PtNi(111) surface do not follow the order. The adsorption energy on top site surface is lowest in the four adsorption site of PtNi(111). It indicates H atom bonds more strongly with a Pt atom than an Ni atom.

3.3. Mechanism of Indole Hydrodenitrogenation

3.3.1. Mechanism of Indole Hydrodenitrogenation on the Ni(111) and Pt(111) Surfaces

Elementary steps of indole hydrodenitrogenation on the Ni(111) and Pt(111) surfaces divided into 20 steps are shown in Figures 6 and 7, respectively. The potential energy profiles of indole hydrodenitrogenation on the Ni(111) and Pt(111) surfaces are shown in Figures 8 and 9, respectively. The corresponding activation energies and reaction energies

are listed in Table 3. The reaction pathway of indole hydrogenation is determined in two parts: Ring hydrogenation and heterocyclic ring opening.



Figure 6. Mechanism of indole hydrogenation on Ni(111) surface: (a) to (t) represent Step 1 to Step 20.

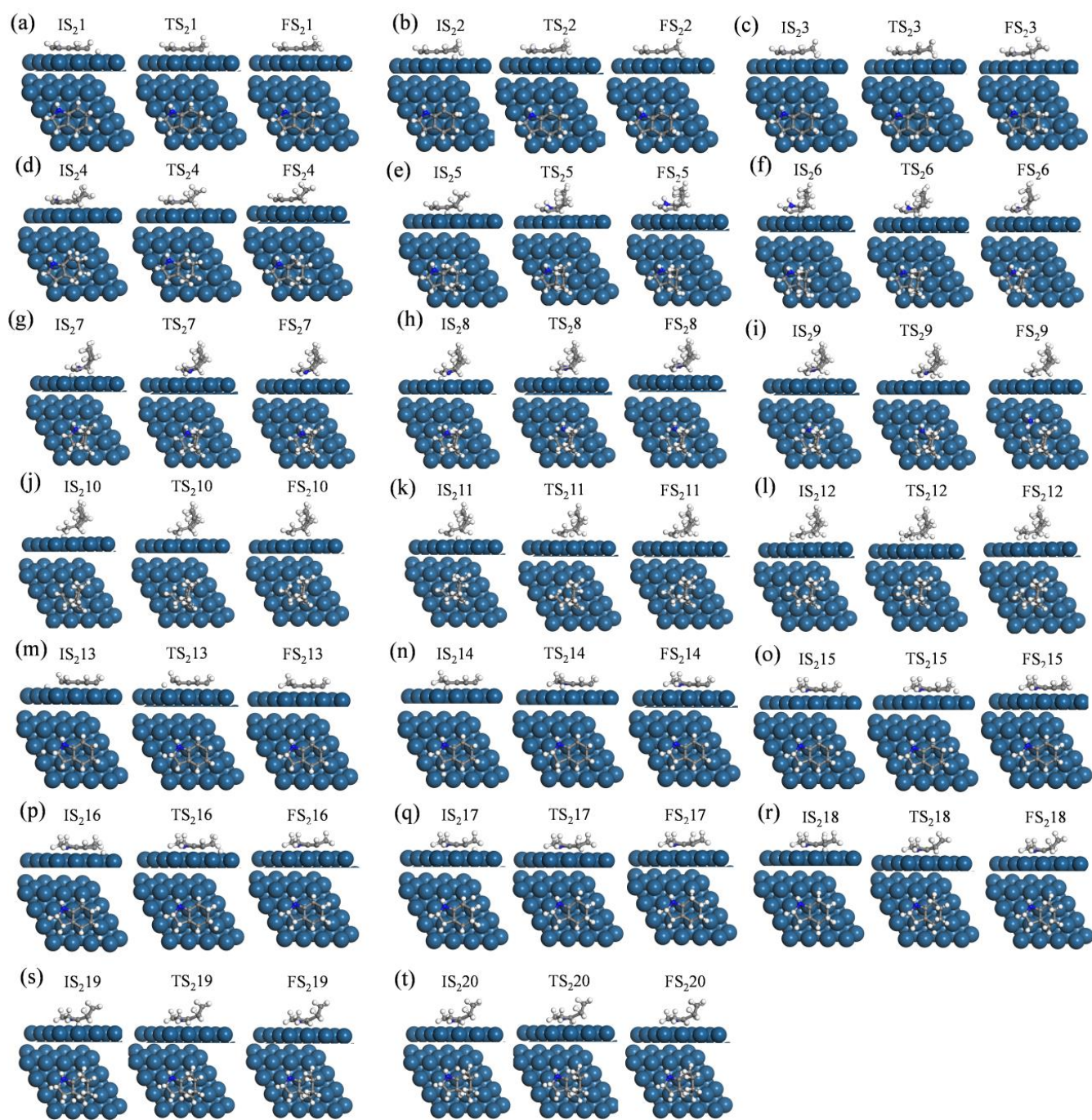


Figure 7. Mechanism of indole hydrodenitrogenation on Pt(111) surface: (a) to (t) represent Step 1 to Step 20.

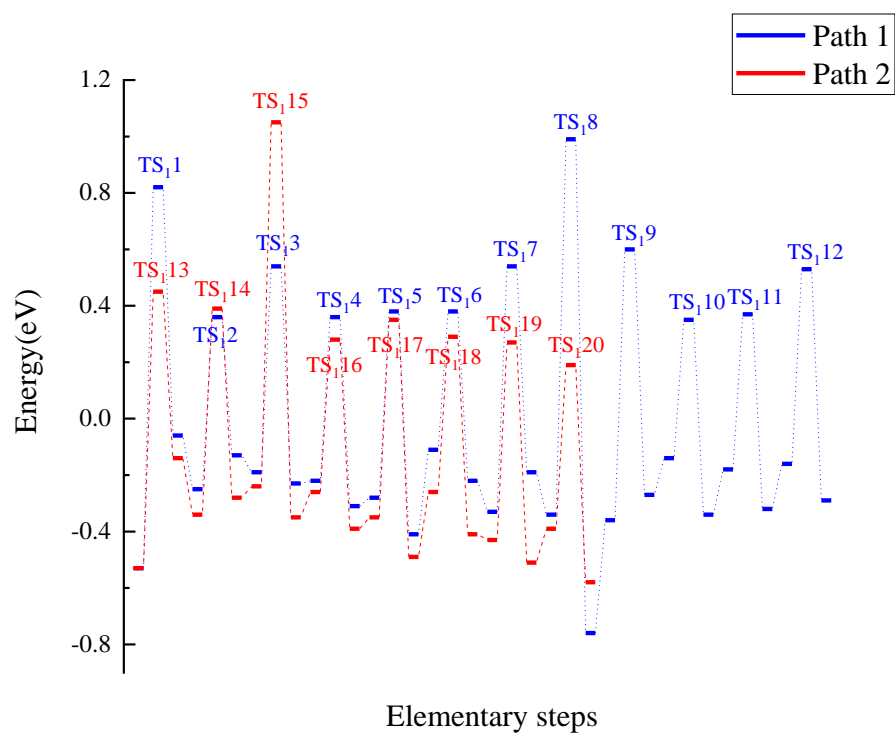


Figure 8. Potential energy profiles of indole hydrodenitrogenation on Ni(111) surface.

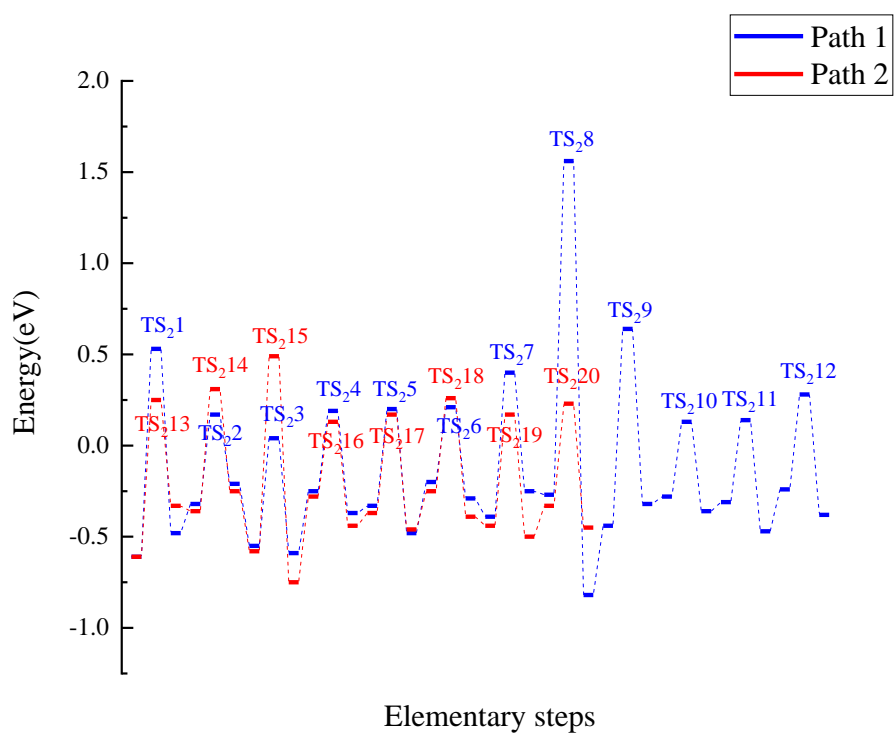


Figure 9. Potential energy profiles of indole hydrodenitrogenation on Pt(111) surface.

Table 3. Activation energies and reaction energies of indole hydrodenitrogenation on M(111) surface.

No.	Elementary Steps	Ni(111)		Pt(111)		NiPt(111)		PtNi(111)	
		E _a	E _{rxn}						
Step 1	C ₈ H ₇ N* + H* → C ₈ H ₈ N*	1.35	0.47	1.14	0.13	1.11	0.26	1.09	0.42
Step 2	C ₈ H ₈ N* + H* → C ₈ H ₉ N*	0.61	0.12	0.49	0.11	0.51	0.14	0.51	0.12
Step 3	C ₈ H ₉ N* + H* → C ₈ H ₁₀ N*	0.73	−0.04	0.59	−0.04	0.55	−0.01	0.52	−0.08
Step 4	C ₈ H ₁₀ N* + H* → C ₈ H ₁₁ N*	0.58	−0.09	0.44	−0.12	0.34	−0.10	0.31	−0.11
Step 5	C ₈ H ₁₁ N* + H* → C ₈ H ₁₂ N*	0.66	−0.13	0.53	−0.15	0.52	−0.16	0.55	−0.09
Step 6	C ₈ H ₁₂ N* + H* → C ₈ H ₁₃ N*	0.49	−0.11	0.41	−0.09	0.38	−0.05	0.43	−0.12
Step 7	C ₈ H ₁₃ N* + H* → C ₈ H ₁₄ N*	0.87	0.14	0.79	0.14	0.77	0.17	0.72	0.11
Step 8	C ₈ H ₁₄ N* + H* → C ₈ H ₁₅ N*	1.33	−0.42	1.83	−0.55	1.60	−0.57	1.15	−0.57
Step 9	C ₈ H ₁₅ N* + H* → C ₈ H ₁₃ + NH ₃ *	0.96	0.09	1.08	0.12	0.98	0.09	0.91	0.05
Step 10	C ₈ H ₁₃ + H* → C ₈ H ₁₄ *	0.49	−0.20	0.41	−0.08	0.40	−0.06	0.39	−0.17
Step 11	C ₈ H ₁₄ * + H* → C ₈ H ₁₅ *	0.55	−0.14	0.45	−0.16	0.48	−0.2	0.46	−0.12
Step 12	C ₈ H ₁₅ * + H* → C ₈ H ₁₆ *	0.53	−0.13	0.52	−0.14	0.50	−0.11	0.54	−0.16
Step 13	C ₈ H ₇ N* + H* → C ₈ H ₈ N*	0.98	0.39	0.86	0.28	0.84	0.35	0.90	0.30
Step 14	C ₈ H ₈ N* + H* → C ₈ H ₉ N*	0.73	0.06	0.67	0.11	0.63	0.09	0.60	0.14
Step 15	C ₈ H ₉ N* + H* → C ₈ H ₁₀ N*	1.29	−0.11	1.07	−0.17	1.00	−0.13	1.03	−0.21
Step 16	C ₈ H ₁₀ N* + H* → C ₈ H ₁₁ N*	0.54	−0.13	0.41	−0.16	0.33	−0.14	0.39	−0.19
Step 17	C ₈ H ₁₁ N* + H* → C ₈ H ₁₂ N*	0.70	−0.14	0.54	−0.09	0.51	−0.17	0.59	−0.11
Step 18	C ₈ H ₁₂ N* + H* → C ₈ H ₁₃ N*	0.55	−0.15	0.51	−0.14	0.50	−0.17	0.56	−0.23
Step 19	C ₈ H ₁₃ N* + H* → C ₈ H ₁₄ N*	0.64	−0.08	0.61	−0.06	0.56	−0.11	0.63	−0.12
Step 20	C ₈ H ₁₄ N* + H* → C ₈ H ₁₅ N*	0.58	−0.19	0.56	−0.12	0.54	−0.21	0.61	−0.29

3.3.2. Ring Hydrogenation

Ring hydrogenation includes benzene ring hydrogenation first (Path 1) and heterocyclic ring hydrogenation first (Path 2). On the Ni(111) surface in Figure 6, the reaction of benzene ring hydrogenation is first divided into six elementary steps. The first elementary step starts from indole adsorption configuration in Figure 2b. The C atoms in the benzene ring are attacked by an H atom step by step. In the first hydrogenation step, the destruction of conjugation in the benzene ring shows high activation energy of 1.35 eV. After the first hydrogenation step is complete, the following hydrogenation steps proceed more easily with lower activation energies than the first step. The activation energies of step 2 to step 6 are in the range between 0.58 and 0.73 eV. The activation energy of step 3 is higher than the other steps because the benzene ring intermediate transforms from slab conformation to boat conformation, requiring more energy. According to the activation energies of Path 1 on the Ni(111) surface, step 1, with activation energy of 1.35 eV, is the rate-determining step in Path 1.

The reaction of heterocyclic ring hydrogenation first on the Ni(111) surface is divided into eight elementary steps, which are shown from step 13 to step 20. The first elementary step starts from the indole adsorption configuration in Figure 2c. The C atoms in the heterocyclic ring are attacked by an H atom step by step. Because of π conjugation effect in benzene ring, the activation energy of step 15 with 1.29 eV is the highest in Path 2. This indicates step 15 is the rate-determining step in Path 2. Compared to Path 1, the activation energy of the rate-determining step in Path 2 is lower than that in Path 1, which indicates the reaction pathway of heterocyclic ring hydrogenation first is easier to proceed than the reaction pathway of benzene ring hydrogenation first.

On the Pt(111) surface in Figure 7, the benzene ring hydrogenation first steps (Path 1) is similar to the steps on the Ni(111) surface. The activation energy of step 1 on the Pt(111) surface is 1.14 eV, which also is highest in the benzene ring hydrogenation. Compared to that on the Ni(111) surface, the activation energy of step 1 on the Pt(111) surface is lower because Pt acts as an active hydrogen supplier which has a promotional effect for hydrogenation [3]. Similar to that on the Ni(111) surface, the activation energies of follow hydrogenation steps on Pt(111) also are lower than the first step. The activation energies of the step 2 to step 6 range between 0.44 and 0.59 eV. All the activation energies of benzene

ring hydrogenation on the Pt(111) surface are lower than that on the Ni(111) surface, which indicates that the Pt(111) surface is favorable for benzene ring hydrogenation.

The heterocyclic ring hydrogenation first steps (Path 2) on the Pt(111) surface is close to that on the Ni(111) surface. Path 2 also includes eight elementary steps, in which step 15, with highest activation energy, is the rate-determining step in Path 2. Compared to the activation energies of Path 1 on the Pt(111) surface, the activation energies of Path 2 are lower. It indicates indole hydrogenation prefers heterocyclic ring hydrogenation first on the Pt(111) surface.

3.3.3. Heterocyclic Ring Opening

For heterocyclic ring opening on the Ni(111) surface, the elementary steps are shown from step 7 to step 12 in Figure 6. In step 7, H atom adsorbs in the hcp site and attacks the C atom in the heterocyclic ring further, in order to weaken the C-N bond. In step 8, the H atom attacks the N atom in the heterocyclic ring and forms an N-H bond, which results in heterocyclic ring opening. In step 9, the H atom continues to attack the N atom in order to achieve denitrogenation. In step 10 to step 12, H atoms hydrogenate one by one to form alkane. The activation energy of step 8 is 1.33 eV. This activation energy is lower than that of step 1 with 1.35 eV, while it is higher than that of step 15 with 1.29 eV. It indicates step 8 is the rate-determining step of indole hydrodenitrogenation.

For heterocyclic ring opening on the Pt(111) surface, the configuration of elementary steps is similar to that on the Ni(111) surface. However, the activation energies of heterocyclic ring opening on the Pt(111) surface is higher than that on the Ni(111) surface. The activation energy of step 8 on the Pt(111) surface is 1.83 eV, which is higher than that of 1.33 eV on the Ni(111) surface. This result indicates that heterocyclic ring opening prefers to proceed on the Ni(111) surface. In addition, the activation energy of step 8 is the highest from step 1 to step 20, which indicates step 8 is the rate-determining step of indole hydrodenitrogenation.

As mentioned above, it suggests that ring hydrogenation prefers to proceed on the Pt(111) surface while heterocyclic ring opening prefers to proceed on the Ni(111) surface. According to the calculation result, we further study indole hydrodenitrogenation on the NiPt(111) surface and the PtNi(111) surface in order to investigate the bimetallic effect. In the next study, we continue to investigate indole hydrodenitrogenation from the two parts of ring hydrogenation and heterocyclic ring opening. The mechanisms of indole hydrodenitrogenation on the NiPt(111) surface and the PtNi(111) surface are shown in Figures 10 and 11, respectively. The potential energy profiles of indole hydrodenitrogenation on the NiPt(111) surface and PtNi(111) are shown in Figures 12 and 13, respectively.

3.3.4. Ring Hydrogenation

Ring hydrogenation also is divided into benzene ring hydrogenation first (Path 1) and heterocyclic ring hydrogenation first (Path 2). On the NiPt(111) surface in Figure 10, the elementary steps of benzene ring hydrogenation first (Path 1) are determined as six steps, which is similar to that on the Pt(111) surface. The N atom in the heterocyclic ring prefers to adsorb on the top site of the Ni atom in the NiPt(111) surface. In addition, the activation energies of benzene ring hydrogenation on the NiPt(111) surface is also close to that on the Pt(111) surface. The rate-determining step of benzene ring hydrogenation is also step 1, with activation energy of 1.11 eV. The activation energies of step 2 to step 6 are in the range between 0.34 and 0.55 eV, which are lower than that of step 1. In addition, the activation energies of six elementary steps on the NiPt(111) surface are all lower than that on the Pt(111) surface, which suggests Ni doping in the Pt(111) surface is positive for benzene ring hydrogenation.

The elementary steps of heterocyclic ring hydrogenation first (Path 2) on the NiPt(111) surface is from step 13 to step 20. The configurations of each elementary step on the NiPt(111) surface are similar to that on the Pt(111) surface. The activation energy of step 15

is 1.00 eV, which is the highest in Path 2. Therefore, step 15 is the rate-determining step on the NiPt(111) surface.

On the PtNi(111) surface in Figure 11, the configurations and activation energies of elementary steps are similar to that on the Ni(111) surface. H atom prefers to adsorb on the top site of Pt atom on the PtNi(111) surface before hydrogenation. The activation energy of step 1 with 1.09 eV is also the highest in the six elementary steps of benzene ring hydrogenation. Compared to that on the Ni(111) surface, the Pt(111) surface and the NiPt(111) surface, the activation energy of step 1 on the PtNi(111) surface is the lowest.

Similar to the other three surfaces, the elementary steps of heterocyclic ring hydrogenation first (Path 2) on the PtNi(111) surface include from step 13 to step 20. Step 15 is a rate-determining step with the highest activation energy in Path 2 on the PtNi(111) surface. Compared to the other three surfaces, the activation energy of step 15 on the PtNi(111) surface is the lowest among the four surfaces. It suggests ring hydrogenation prefers to proceed on the PtNi(111) surface than the others. As reported by other works, the addition of a second metal changes the electronic property of the surface, which results in the difference in adsorption of reactants [23,24].

3.3.5. Heterocyclic Ring Opening

On the NiPt(111) surface in Figure 10, the elementary steps of heterocyclic ring opening are divided from step 7 to step 12. The N atom in the heterocyclic ring prefers to adsorb on the top site of the Ni atom. In step 8, the H atom attacks the N atom in the heterocyclic ring and forms an N-H bond, which results in heterocyclic ring opening. Similar to that on the Pt(111) surface, the activation energy of step 8 with 1.60 eV is highest in indole hydrodenitrogenation. This indicates that step 8 is the rate-determining step of indole hydrodenitrogenation.

On the PtNi(111) surface in Figure 11, the elementary steps of heterocyclic ring opening are similar to that on the NiPt(111) surface. Step 8, C-N bond breaking, is the rate-determining step with the highest activation energy of 1.15 eV in indole hydrodenitrogenation. In addition, the H atom still prefers to adsorb on the top site of the Pt atom before hydrogenation. The other steps of heterocyclic ring opening are easy to proceed with low activation energies ranging between 0.39 and 0.72 eV. Compared to benzene ring hydrogenation, the activation energy of step 8 in heterocyclic ring opening is higher, which indicates step 8 is the rate-determining step of indole hydrodenitrogenation.

According to the calculation results of indole hydrodenitrogenation, the activation energy of rate-determining step on the PtNi(111) surface is the lowest of the the four surfaces. Therefore, the PtNi(111) surface is also favorable for hydrogenation. In summary, indole hydrodenitrogenation is easy to proceed on the PtNi(111) surface. Scheme 1 is shown the reaction pathway of indole hydrodenitrogenation. As mentioned above, the reaction mechanism of indole hydrodenitrogenation includes two possible pathways. Path 1 is benzene ring hydrogenation first (Path 1) and Path 2 is heterocyclic ring hydrogenation first. According to the activation energies of rate-determining steps, Path 2 is easy to proceed, especially, on the PtNi(111) surface. The main reaction pathway: IND→DHIND→OHIND→OECHA→ECH.



Figure 10. Mechanism of indole hydrodenitrogenation on NiPt(111) surface: (a) to (t) represent Step 1 to Step 20.



Figure 11. Mechanism of indole hydrogenation on PtNi(111) surface: (a) to (t) represent Step 1 to Step 20.

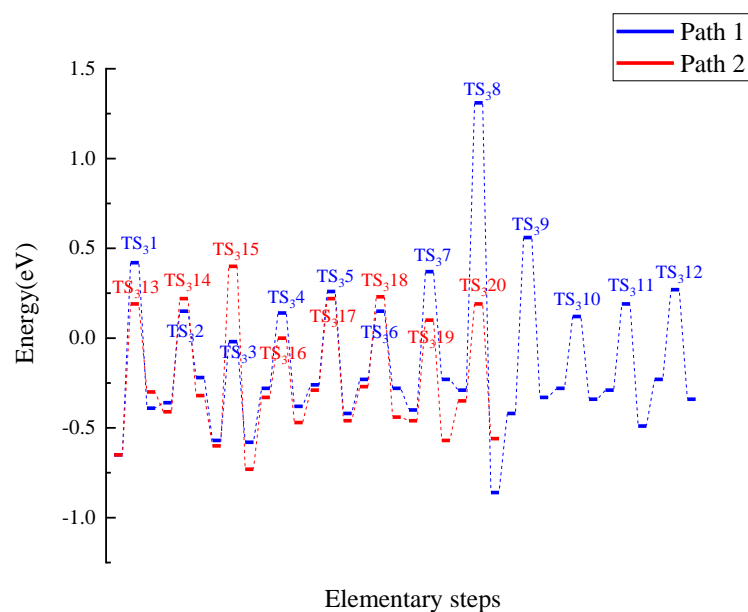


Figure 12. Potential energy profiles of indole hydrodenitrogenation on NiPt(111) surface.

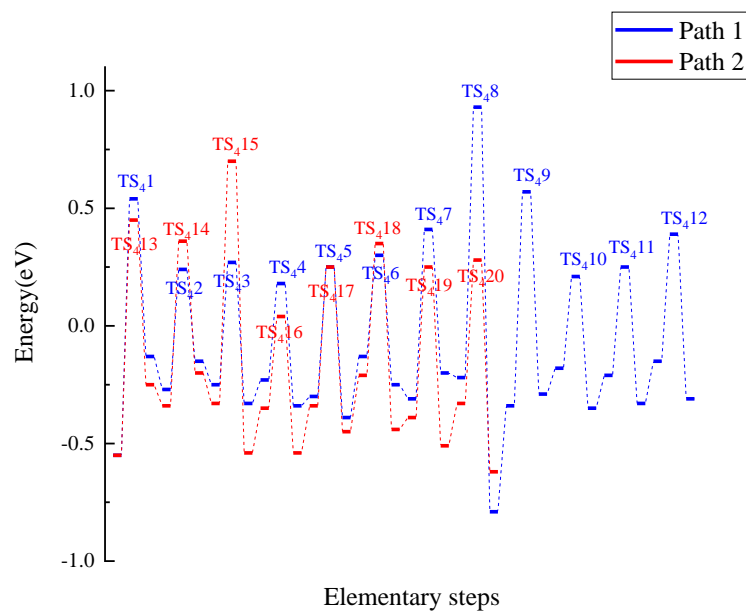
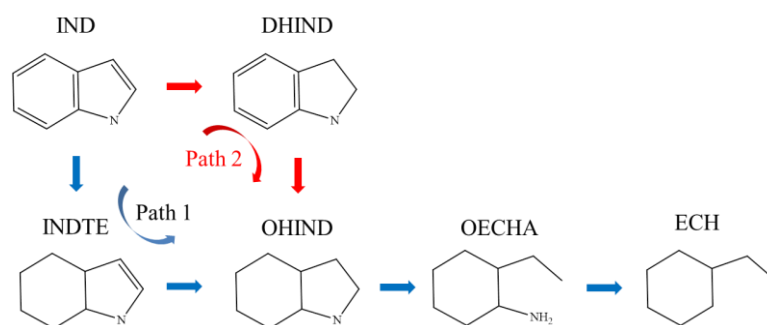


Figure 13. Potential energy profiles of indole hydrodenitrogenation on NiPt(111) surface.



Scheme 1. Proposed reaction pathway for indole hydrodenitrogenation.

4. Conclusions

In this study, DFT was applied to address the reaction mechanisms of indole hydrodenitrogenation on an M slab model. Compared to adsorption energies of reactants and intermediates, a PtNi(111) surface is favorable for indole and intermediates adsorption. In addition, low activation energies of indole hydrodenitrogenation on a PtNi(111) surface result from Pt–Ni bimetallic synergistic effects, which indicates Pt atom doping in an Ni surface is favorable for indole hydrodenitrogenation. The catalytic activities of M surfaces are predicted by DFT calculation, which can support the theoretical guidance for the experiments of indole hydrodenitrogenation.

Author Contributions: Conceptualization, C.W.; methodology, C.W.; software, C.W.; validation, C.W. and H.S.; formal analysis, J.C.; investigation, L.Z.; resources, H.S.; data curation, Y.H.; writing—original draft preparation, H.C.; writing—review and editing, C.W.; visualization, Z.Z.; supervision, C.W.; project administration, C.W.; funding acquisition, H.S. All authors have read and agreed to the published version of the manuscript.

Funding: This research received no external funding.

Institutional Review Board Statement: Not applicable.

Informed Consent Statement: Not applicable.

Data Availability Statement: Exclude this statement.

Acknowledgments: We are grateful for financial support from the University of Science and Technology Liaoning. We also thank the High-Performance Computing Center of China Pharmaceutical University for providing us computational time.

Conflicts of Interest: The authors declare no conflict of interest.

References

1. Gonzalez, C.; Marin, P.; Diez, F.V.; Ordonez, S. Hydrodeoxygenation of Acetophenone over Supported Precious Metal Catalysts at Mild Conditions: Process Optimization and Reaction Kinetics. *Energy Fuels* **2015**, *29*, 8208–8215. [[CrossRef](#)]
2. Ledesma, B.C.; Anunziata, O.A.; Beltramone, A.R. HDN of indole over Ir-modified Ti-SBA-15. *Appl. Catal. B-Environ.* **2016**, *192*, 220–233. [[CrossRef](#)]
3. Infantes-Molina, A.; Romero-Perez, A.; Finocchio, E.; Busca, G.; Jimenez-Lopez, A.; Rodriguez-Castellon, E. HDS and HDN on SBA-supported RuS₂ catalysts promoted by Pt and Ir. *J. Catal.* **2013**, *305*, 101–117. [[CrossRef](#)]
4. Liu, J.; Li, W.-Y.; Feng, J.; Gao, X. Molecular insights into the hydrodenitrogenation mechanism of pyridine over Pt/ γ -Al₂O₃ catalysts. *Mol. Catal.* **2020**, *495*. [[CrossRef](#)]
5. Gulkova, D.; Yoshimura, Y.; Vit, Z. Mesoporous silica-alumina as support for Pt and Pt-Mo sulfide catalysts: Effect of Pt loading on activity and selectivity in HDS and HDN of model compounds. *Appl. Catal. B-Environ.* **2009**, *87*, 171–180. [[CrossRef](#)]
6. Colman, R.d.C.; Scaramelo Baldanza, M.A.; Schmal, M. Influence of Mo Species on the Pt/NaY Catalyst and the Effect of Sulfur Content on the Hydrodenitrogenation Reaction. *J. Phys. Chem. C* **2010**, *114*, 18501–18508. [[CrossRef](#)]
7. Peeters, E.; Cattenot, M.; Geantet, C.; Breyse, M.; Zotin, J.L. Hydrodenitrogenation on Pt/silica-alumina catalysts in the presence of H₂S: Role of acidity. *Catal. Today* **2008**, *133*, 299–304. [[CrossRef](#)]
8. Elliott, D.C.; Sealock, L.J.; Baker, E.G. Chemical processing in high-pressure aqueous environments. 2. Development of catalysts for gasification. *Ind. Eng. Chem. Res.* **1993**, *32*, 1542–1548. [[CrossRef](#)]
9. Hirschon, A.S.; Wilson, R.B., Jr.; Laine, R.M. Ruthenium promoted hydrodenitrogenation catalysts. *Appl. Catal.* **1987**, *34*, 311–316. [[CrossRef](#)]
10. Mcvicker, G.B.; Daage, M.; Touvelle, M.S.; Hudson, C.W.; Klein, D.P.; Baird, W.C.; Cook, B.R.; Chen, J.G.; Hantzer, S.; Vaughan, D. Selective Ring Opening of Naphthenic Molecules. *J. Catal.* **2002**, *210*, 137–148. [[CrossRef](#)]
11. Galperin, L.B.; Bricker, J.C.; Holmgren, J.R. Effect of support acid-basic properties on activity and selectivity of Pt catalysts in reaction of methylcyclopentane ring opening. *Appl. Catal. A-Gen.* **2003**, *239*, 297–304. [[CrossRef](#)]
12. Atsumi, R.; Kobayashi, K.; Cui, X.; Nanba, T.; Matsumoto, H.; Matsuda, K.; Tsujimura, T. Effects of steam on toluene hydrogenation over a Ni catalyst. *Appl. Catal. A-Gen.* **2020**, *590*, 117374. [[CrossRef](#)]
13. Ding, D.; Wang, C. Nickel-Catalyzed Reductive Electrophilic Ring Opening of Cycloketone Oxime Esters with Aryl Chlorides. *ACS Catal.* **2018**, *8*, 11324–11329. [[CrossRef](#)]
14. Wang, C.; Zhang, Z.; Liu, K.; Yan, J.; Zhang, T.; Lu, G.; Meng, Q.; Chi, H.; Duan, C. Copper-catalyzed synthesis of indolyl diketones via C-H oxidation/diacylation of indoles with arylglyoxal hydrates. *Org. Biomol. Chem.* **2017**, *15*, 6185–6193. [[CrossRef](#)] [[PubMed](#)]

15. Pan, D.; Chu, J.; Gao, X.; Wang, C.; Meng, Q.; Chi, H.; Dong, Y.; Duan, C.; Zhang, Z. Regioselective N-1 and C-2 diacylation of 3-substituted indoles with arylglyoxal hydrates for the synthesis of indolyl diketones. *Org. Biomol. Chem.* **2018**, *16*, 6998–7003. [[CrossRef](#)] [[PubMed](#)]
16. Wang, C.; Wang, S.; Li, H.; Yan, J.; Chi, H.; Chen, X.; Zhang, Z. Copper-catalyzed decarboxylative C3-acylation of free (N-H) indoles with alpha-oxocarboxylic acids. *Org. Biomol. Chem.* **2014**, *12*, 1721–1724. [[CrossRef](#)]
17. Biller, P.; Ross, A.B. Potential yields and properties of oil from the hydrothermal liquefaction of microalgae with different biochemical content. *Bioresour. Technol.* **2011**, *102*, 215–225. [[CrossRef](#)] [[PubMed](#)]
18. Luo, L.; Liu, S.; Liu, C.; Wang, Y.; Dai, L. High yield of Hydrocarbons from Catalytic Hydrodenitrogenation of Indole Under Hydrothermal Conditions. *Energy Fuels* **2017**, *31*, 12594–12602. [[CrossRef](#)]
19. Dinamarca, R.; Valles, V.; Ledesma, B.; Campos, C.H.; Pecchi, G.; Beltramone, A. Magnetic Fe₃O₄@SiO₂-Pt and Fe₃O₄@SiO₂-Pt@SiO₂ Structures for HDN of Indole. *Materials* **2019**, *12*, 3878. [[CrossRef](#)]
20. Jung, K.T.; Kim, W.B.; Rhee, C.H.; Lee, J.S. Effects of transition metal addition on the solid-state transformation of molybdenum trioxide to molybdenum carbides. *Chem. Mater.* **2004**, *16*, 307–314. [[CrossRef](#)]
21. Liu, X.; Ding, S.; Wei, Q.; Zhou, Y.; Zhang, P.; Xu, Z. DFT insights in to the hydrodenitrogenation behavior differences between indole and quinoline. *Fuel* **2021**, *285*, 119039. [[CrossRef](#)]
22. Piskorz, W.; Adamski, G.; Kotarba, A.; Sojka, Z.; Sayag, C.; Djega-Mariadassou, G. Hydrodenitrogenation of indole over Mo₂C catalyst: Insights into mechanistic events through DFT modeling. *Catal. Today* **2007**, *119*, 39–43. [[CrossRef](#)]
23. Ou, Z.; Ran, J.; Niu, J.; Zhang, Z.; Qin, C. Effect of active site and charge transfer on methane dehydrogenation over different Co doped Ni surfaces by density functional theory. *Int. J. Hydrogen Energy* **2020**, *45*, 31849–31862. [[CrossRef](#)]
24. Zhang, G.; Zhang, X.; Meng, Y.; Zhou, X.; Pan, G.; Ni, Z.; Xia, S. Experimental and Theoretical Investigation into Visible-light-promoted Selective Hydrogenation of Crotonaldehyde to Crotonyl Alcohol using Au-Co,Ni Alloy Nanoparticles Supported Layered Double Hydroxides. *J. Mater. Chem. A* **2018**, *6*, 15839–15852. [[CrossRef](#)]